The 12C(e, e′p) and 12C(e, e′pp) reactions in the Δ-resonance region

Zondervan, A.; de Bever, L.J.; Jans, E.; Konijn, J.; Kruijer, M.; Steijger, J.J.M.; Visschers, J.L.; Countryman, P.J.; Hesselink, W.H.A.; Kalantar-Nayestanaki, N.; Kester, L.J.H.M.; Mitchell, J.H.; Pellegrino, A.; Calarco, J.R.; Hersman, F.W.; Leuschner, M.; Smith, T.P.; Bauer, T.S.; Kelder, M.W.; Giusti, C.; Pacati, F.D.; Ryckebusch, J.; Vanderhaeghen, M.

DOI
10.1016/0375-9474(95)00044-2

Publication date
1995

Published in
Nuclear Physics A

ELSEVIER

Nuclear Physics A 587 (1995) 697–720

NUCLEAR PHYSICS A

The $^{12}C(e, e'p)$ and $^{12}C(e, e'pp)$ reactions in the Δ-resonance region

A. Zondervan [a,1], L.J. de Bever [a], E. Jans [a], J. Konijn [a], M. Kruijer [a], J.J.M. Steijger [a], J.L. Visschers [a,2], P.J. Countryman [b], W.H.A. Hesselink [b], N. Kalantar-Nayestanaki [b,3], L.J.H.M. Kester [b], J.H. Mitchell [b], A. Pellegrino [b], J.R. Calarco [c], F.W. Hersman [c], M. Leuschner [c], T.P. Smith [c], Th.S. Bauer [d], M.W. Kelder [d], C. Giusti [e], F.D. Pacati [e], J. Ryckebusch [f], M. Vanderhaeghen [f]

[a] *National Institute for Nuclear Physics and High-Energy Physics, section K (NIKHEF-K), P.O. Box 41882, 1009 DB Amsterdam, the Netherlands*

[b] *Department of Physics and Astronomy, Free University Amsterdam, De Boelelaan 1081, 1081 HV Amsterdam, the Netherlands*

[c] *Department of Physics, University of New Hampshire, Durham, NH 03824, USA*

[d] *Physics Laboratory, University of Utrecht, P.O. Box 80000, 3508 TA Utrecht, the Netherlands*

[e] *Dipartimento di Fisica Nucleare e Teorica dell'Università Pavia and Istituto Nazionale di Fisica Nucleare, Sezione di Pavia, Italy*

[f] *Institute for Theoretical Physics, Proeftuinstraat 86, B-9000 Gent, Belgium*

Received 28 December 1994; revised 9 February 1995

Abstract

Coincidence cross sections for the $^{12}C(e, e'pp)$ and $^{12}C(e, e'p)$ reactions have been measured in the Δ-resonance region. The $^{12}C(e, e'pp)$ reaction has been measured at three different angular settings of the proton detectors to investigate the angular correlation between the emitted protons. The data, which have a low statistical accuracy, are compared with a calculation based on the direct-knockout mechanism, which includes one- and two-body currents. NN-correlations are accounted for via a correlation function, Δ-excitation via a two-body current and final-state interactions of the emitted protons via an optical potential. The $^{12}C(e, e'p)$ data, taken at large proton-emission angles, cover the region of high missing-energy values (145–275 MeV). The data

[1] Present address: Centre for Isotope Research, University of Groningen, Nijenborgh 4, 9747 AG Groningen, the Netherlands.

[2] On leave of absence at CERN/ECP, CH-1211 Geneva 23, Switzerland.

[3] Present address: KVI, Zernikelaan 25, 9747 AA Groningen, the Netherlands.

SSDI 0375-9474(95)00044-5

are compared to results of a calculation taking into account meson exchange, intermediate Δ-excitation and pion production. This comparison shows that there is ample evidence for processes leading to multi-nucleon knockout.

Keywords: NUCLEAR REACTIONS ^{12}C(e, e'p), (e, e2p), $E \approx$ resonance; measured six-fold, nine-fold differential σ; deduced reaction mechanism. Model comparison.

1. Introduction

The energy spectrum of electrons scattered off a nucleus exhibits a broad structure centred around the energy transfer $\omega \approx Q^2/2m_N$, where Q is the four-momentum transfer and m_N the nucleon mass. This structure corresponds to quasi-free scattering (QFS), a process in which the virtual photon is absorbed by one nucleon which subsequently leaves the nucleus. At energy transfers beyond the QFS region a second structure develops, which is associated with the excitation of one of the target nucleons into a Δ. A free Δ decays either to a nucleon and a pion or, with a probability of 0.6%, to a nucleon and a photon. In the presence of other nucleons the Δ can also de-excite via the $\Delta + N \rightarrow N + N$ channel. Due to the large excess of available kinetic energy after this de-excitation, the two nucleons most likely leave the nucleus. More complicated processes, such as final-state interactions (FSI), take place as well and may lead to the emission of more than two nucleons. The two mentioned structures – the QFS peak and the Δ-resonance – are separated from each other by the so-called "dip" region, where most theoretical calculations fail to reproduce the inclusive electron-scattering cross section [1,2]. Apparently, the combination of the QFS process, the tail of Δ-production, the onset of nonresonant pion production and effects such as FSI and meson-exchange currents (MEC) is insufficient to reproduce the experimental results. Therefore, additional mechanisms have been invoked, such as nucleon–nucleon correlations [3–5] and six-quark structures [6].

Whereas QFS is reasonably well understood both theoretically and experimentally, little is known about the nuclear response to virtual photons in the dip and Δ-resonance regions. The simple fact that much more energy is transferred than in the case of the QFS process can lead to final states with at least two fast hadrons, either two nucleons or a nucleon and a pion. In order to obtain kinematically complete information, the scattered electron must, therefore, be detected in coincidence with at least two emitted particles. Results of such triple-coincidence experiments have not yet been published. Besides double- and triple-coincidence data with tagged photons [7,8], only a few semi-exclusive measurements have been performed with virtual photons. Among them are the studies of Marchand et al. [9] of the reaction ^{3}He(e, e'p) and of Baghaei et al. [10] of the reaction ^{12}C(e, e'p). In both studies evidence was obtained for reaction mechanisms in which two nucleons are involved.

The (e, e'NN) reaction is a suitable tool to investigate the two-body aspects of nuclear structure [11]. It gives access to the two-body density and thus to dynamical short-range correlations (SRC), which are generated by violent NN collisions at short internucleon distances and thus go beyond an independent particle-model description of the nucleus.

In principle both the (e, e′pp) and the (e, e′pn) reactions can be used. The (e, e′pp) cross section is expected to be about an order of magnitude lower than the (e, e′pn) cross section [12,13]. However, if one wants to investigate SRCs, the (e, e′pp) reaction has distinct advantages. Spin–isospin selection rules strongly suppress de-excitation of the ΔN-system into a pp-pair and, at lowest order, coupling to charged MECs does not contribute for a pp-pair. Therefore, the transverse response, which is largely determined by MECs and Δ-excitation, is most important for the (e, e′pn) cross section and is strongly suppressed in the (e, e′pp) case. On the contrary, the longitudinal response, which is particularly sensitive to SRCs, is expected to dominate the cross section of the (e, e′pp) reaction, which can thus be considered as a preferential candidate for the search for SRC effects. This has been exploited in a calculation by Laget for ^{3}He [13,14]. The sensitivity of electron-induced two-proton knockout to SRCs has been shown in a calculation by Giusti and Pacati for ^{16}O and ^{40}Ca [15].

The first goal in exploring this new field of two-nucleon knockout is to understand the general features of the emission processes and to establish the similarities and differences with such processes induced by other probes. In this first investigation of the triple-coincidence reaction with electrons we have chosen to measure the reaction ^{12}C(e, e′pp), where the protons are detected in the scattering plane. Besides being more suited to investigate SRC effects, a triple-coincidence measurement involving only charged particles is also easier to accomplish than the detection of electron–proton–neutron coincidences. Evidently, future studies must involve the presumably dominant but experimentally more difficult pn-channel as well. The aim of the measurement reported here is to establish the method of triple-coincidence experiments, to determine the ^{12}C(e, e′pp) reaction cross section in the Δ-resonance region and to investigate the angular correlation of the two emitted protons. Conservation of momentum dictates that in all cases where two nucleons are involved, they are emitted back-to-back in the centre-of-mass frame of the projectile plus the initial two-particle system, irrespective of the underlying reaction mechanism. Conversely, a 180° correlation is a signature of a two-particle process. For nuclei with $A > 2$, Fermi motion of the nucleons and FSIs with the residual nucleus will smear out this 180° correlation. However, pion-absorption measurements have shown [16,17] that the distinct angular correlation is not washed away by such effects. This correlation is valid for any process in which exactly two nucleons are emitted. Although its observation does not allow one to draw conclusions concerning the underlying dynamics, it indicates that a process involving two nucleons is dominant.

In Section 2, the choice for the (e, e′pp) kinematical conditions is discussed and a short description of the electron and proton detectors and their calibration is given. Semi-exclusive (e, e′p) events, with missing-energy values above the two-nucleon emission and the pion-production thresholds, have been measured simultaneously with the (e, e′pp) events. In this paper we only discuss the (e, e′p) data measured at backward proton-emission angles. Section 3 starts with the procedure for the analysis of the (e, e′p) data of which the results are expressed in terms of six-fold differential cross sections. Next, a new approach towards the analysis of triple-coincidence data with low

statistics is presented and the resulting values for the present ^{12}C(e, e′pp) experiment are given. In Section 4, estimates of the effect of radiative processes and nucleon rescattering are presented. Contributions from quasi-free (e, e′p) an (e, e′pπ) at backward angles are discussed using results of the Monte Carlo code ENIGMA which uses a plane-wave formalism. The semi-exclusive (e, e′p) data are compared with predictions of an unfactorized approach which accounts for MECs, intermediate Δ-excitation and pion production. In Section 5, the interpretation of (e, e′pp) data is discussed and the experimental results are compared with predictions from a model calculation for two-nucleon knockout which includes one- and two-body currents. Finally, in Section 6, the summary and conclusions of the present work are given.

2. Kinematics and experimental setup

The measurements have been performed with the 1% duty-factor electron accelerator MEA at NIKHEF. The experimental setup consisted of a magnetic spectrometer for the detection of the scattered electrons and of two plastic-scintillator arrays for the detection of the emitted protons. The scintillation detectors were specially designed and constructed for triple-coincidence (e, e′pp) studies with MEA. They each cover a solid angle of 39 msr, have a large energy acceptance and can be operated up to a peak singles count rate of 15 MHz. Details of the experimental setup will be given in subsection 2.3. The reconstruction of the momentum vector of the detected particles from the raw data is described in Subsection 2.4, followed by an outline of the coincidence electronics and the data acquisition in Subsection 2.5. The most relevant kinematical variables are introduced in Subsection 2.1. Then we discuss in Subsection 2.2 the choice of the kinematical conditions.

2.1. Kinematical variables

The kinematics of the quasi-free two-nucleon knockout reaction A(e, e′pN)$(A-2)$ is shown in Fig. 1 in a simplified picture. Initially, the two nucleons have momenta $\boldsymbol{k}_{\mathrm{p}}$ and $\boldsymbol{k}_{\mathrm{N}}$. The kinematics of the initial state of such a system can be described in terms of the relative motion between the two nucleons $\boldsymbol{k}_{\mathrm{rel}} \equiv \frac{1}{2}(\boldsymbol{k}_{\mathrm{p}} - \boldsymbol{k}_{\mathrm{N}})$ and of the centre-of-mass motion of the two-nucleon pair $\boldsymbol{k}_{\mathrm{c.m.}} \equiv \boldsymbol{k}_{\mathrm{p}} + \boldsymbol{k}_{\mathrm{N}}$. The three-momentum $\boldsymbol{q}$ and energy ω are transferred to the pair, and the two nucleons leave the nucleus with momenta $\boldsymbol{p}_{\mathrm{p}}$ and $\boldsymbol{p}_{\mathrm{N}}$. For clarity, the $(A-2)$ spectator system is chosen to be at rest ($\boldsymbol{k}_{\mathrm{c.m.}} = 0$) in the kinematic picture of Fig. 1. Also, FSIs are neglected.

Fig. 1 corresponds to the extreme case where the virtual photon couples to the proton p only and thus

$$\boldsymbol{p}_{\mathrm{N}} = \boldsymbol{k}_{\mathrm{N}}, \tag{1a}$$

$$\boldsymbol{k}_{\mathrm{rel}} = \tfrac{1}{2}(\boldsymbol{k}_{\mathrm{p}} - \boldsymbol{k}_{\mathrm{N}}) = \tfrac{1}{2}(\boldsymbol{p}_{\mathrm{p}} - \boldsymbol{q} - \boldsymbol{p}_{\mathrm{N}}). \tag{1b}$$

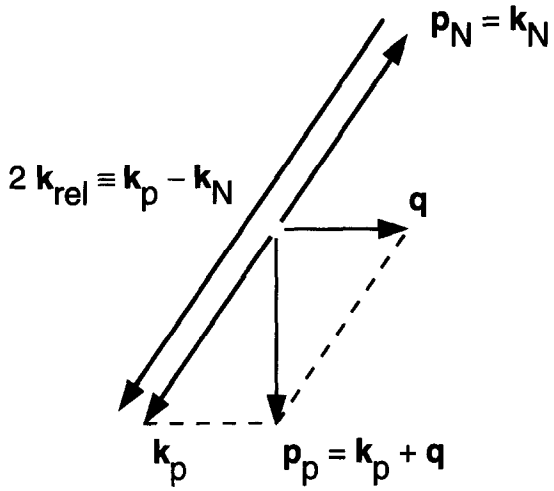

Fig. 1. Simplified picture of the kinematics of the two-nucleon knockout reaction A(e, e′pN)$(A-2)$ in the laboratory frame in terms of the initial momenta $\boldsymbol{k}$ and the final momenta $\boldsymbol{p}$. In this case the momentum $\boldsymbol{q}$ is transferred to the proton only. The centre-of-mass motion $\boldsymbol{k}_{\mathrm{c.m.}}$ of the NN-pair and final-state interactions are neglected.

The other extreme case, where the virtual photon couples to the nucleon N only, corresponds to

$$\boldsymbol{p}_{\mathrm{p}} = \boldsymbol{k}_{\mathrm{p}}, \tag{2a}$$

$$\boldsymbol{k}_{\mathrm{rel}} = \tfrac{1}{2}\left(\boldsymbol{k}_{\mathrm{p}} - \boldsymbol{k}_{\mathrm{N}}\right) = \tfrac{1}{2}\left[\boldsymbol{p}_{\mathrm{p}} - \left(\boldsymbol{p}_{\mathrm{N}} - \boldsymbol{q}\right)\right]. \tag{2b}$$

Given the same values of the observables $\boldsymbol{q}$ and $\boldsymbol{p}_{\mathrm{p}}$, these cases correspond with different values of $\boldsymbol{k}_{\mathrm{rel}}$. In general, many initial states, each of which is characterized by its own values of $\boldsymbol{k}_{\mathrm{c.m.}}$ and $\boldsymbol{k}_{\mathrm{rel}}$, can lead to the same final state characterized by the observables $\boldsymbol{q}$ and $\boldsymbol{p}_{\mathrm{p}}$. Evidently, the probabilities of such initial states can differ considerably. $\boldsymbol{k}_{\mathrm{c.m.}}$ is for all cases equal to $\boldsymbol{p}_{\mathrm{p}} + \boldsymbol{p}_{\mathrm{N}} - \boldsymbol{q}$, whereas $\boldsymbol{k}_{\mathrm{rel}}$ differs. Therefore, $\boldsymbol{k}_{\mathrm{rel}}$ is not an observable. In other words, one cannot distinguish how the virtual photon coupled to the two-nucleon system.

2.2. Choice of kinematical conditions

The kinematical conditions for the experiment were constrained by the characteristics of the electron accelerator, the allowable singles rates in the detectors and the spatial limitations of the three-detector setup. The final choice was mainly determined by the expected correlation between the emission angles of the two protons in the (e, e′pp) reaction, while a lower priority was given to the measurement of the ^{12}C(e, e′p) reaction.

The beam energy $E_{\mathrm{e}} = 509$ MeV was the highest possible energy for this experiment. The scattered electrons were detected at $\theta_{\mathrm{e}'} = -27°$, which was the smallest angle accessible for the magnetic spectrometer. The values for the momentum and energy

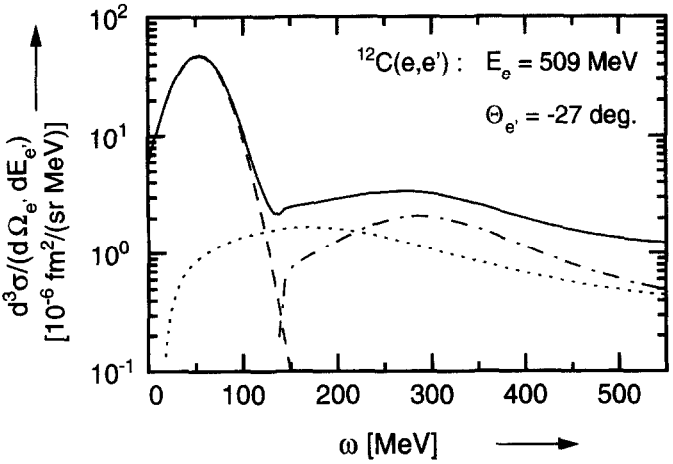

Fig. 2. Prediction of the ^{12}C(e, e') cross section by the QFS code versus the energy transfer ω at the beam energy and electron-spectrometer angle of the present experiment. The dashed, dotted and dash-dotted curves represent the cross section due to quasi-elastic knockout, two-nucleon knockout and Δ-excitation, respectively. The solid curve is the incoherent sum of these processes.

transfer $(q, \omega) = (343\ \text{MeV}/c,\ 310\ \text{MeV})$ are completely determined by the beam energy and the electron-scattering angle once the invariant mass $W = 2160$ MeV for the $\gamma^* + 2\text{p} \rightarrow \Delta^+ + \text{p}$ process is fixed. The inclusive ^{12}C(e, e') cross section, as calculated with the code QFS [18] for these kinematical conditions, is shown in Fig. 2. Clearly, at $\omega = 310$ MeV the excitation of the Δ-resonance dominates the reaction. The momentum transfer is directed almost parallel to the beam ($\theta_q = 15°$) due to the low energy of the scattered electron relative to the beam energy.

To probe the nucleus at relatively low values of $\boldsymbol{k}_{\text{rel}}$, where the maximum cross section is expected, one should detect one proton in a direction as close to the momentum-transfer vector as possible. However, the use of a plastic-scintillator array for proton detection sets a lower limit on the detection angle. The upper limit on the allowable singles rate and a practical lower limit on the luminosity excluded measurements at angles $|\theta| < 55°$.

A determination of the most appropriate positions of detector P1 requires an estimate of the angular correlation between the emission angles of the two hadrons in the laboratory (lab) frame. The two-nucleon knockout process has been simulated with the Monte Carlo computer code ENIGMA [19]. A short description of this code is given in Subsection 4.4, where a simulation of the semi-exclusive ^{12}C(e, e'p) data is presented. Here, only those aspects of the simulation are discussed which are relevant for an estimate of the width and location of the angular correlation.

The energy- and angular-correlation patterns in the ^{12}C(e, e'pp) reaction are estimated from a simulation of the reaction ^{12}C(e, e'pn)^{10}B* assuming the quasi-free knockout of a pn-pair. The excitation-energy spectrum of the recoil nucleus is assumed to be constant up to 60 MeV and equal to zero for higher values. The momentum of the pn-pair relative to the residual nucleus is constructed from a vectorial sum of the

momenta of these nucleons. They are assumed to move independently according to gaussian distributions centred around $k_p = 0$ MeV/c and with a variance $\sigma = 110$ MeV/c, a value that results in a reasonable nucleon-momentum distribution [20].

For this simulation the electron kinematics and the angle of one proton were fixed at the above-mentioned central (i.e. detector) values. The resulting angular distribution of the backward proton is approximately gaussian shaped (FWHM = 55°) and centred around $-90°$, which is close to the conjugate angle. On the basis of this distribution and the fact that the smallest possible angle between the central lines of the magnetic spectrometer and a scintillation detector is 53°, detector P1 has been placed at $\theta_1 = -80°$, $-96°$ and $-120°$. These settings roughly cover the expected angular-correlation pattern. In addition, data have been collected at $\theta_1 = -108°$ and $\theta_2 = 90°$ in order to cover more completely the angular distribution of the emitted proton of the semi-exclusive ^{12}C(e, e'p) reaction. The expected rate for (e, e'pp) events in this setting is low since it deviates strongly from the back-to-back pattern that dominates a two-proton-emission reaction mechanism. The energy acceptances of the proton detectors were matched to the predicted energy ranges by using absorbers, as will be discussed in the next subsection.

2.3. Electron and proton detectors

The quadrupole–dipole–quadrupole (QDQ) magnetic spectrometer, used for the detection of the scattered electrons, has an effective momentum acceptance of 9% and a solid angle of 12.2 msr. The focal-plane detection system consists of four multi-wire drift chambers and two layers of trigger scintillators [21].

The proton detection system consists of two almost identical, segmented plastic-scintillator arrays. Their design specifications, along with a description of the VME-based flash electronics and first performance results are described in detail in Ref. [22]. Both detectors are designed for use at a distance of about 75 cm between the interaction point and the first scintillator layer. The position of impact is determined by a two-dimensional hodoscope. The angular resolution is approximately one degree in both directions. The vertical and horizontal acceptances are 9.8° and 13.4°, respectively, resulting in a geometrical solid angle of 39 msr. The energy acceptances for protons detected in detectors P1 and P2 are 25–158 and 37–198 MeV, respectively. The segmentation has been chosen such that the singles rates in all elements are comparable. Low-energy electrons and other particles with ranges on the order of millimetres are stopped in the hodoscope and do not produce a trigger. Fast electrons are suppressed by appropriate discriminator thresholds of the counters that constitute the trigger condition.

Test runs at backward angles indicated that a thin lead (Pb) absorber placed between the scattering chamber and the proton detector reduces the singles rate significantly, allowing a proportional increase of the luminosity. Because of the expected low triples count rate, it was decided to sacrifice low-energy protons for higher luminosity. Therefore, a 1 mm thick absorber was installed in front of the hodoscope of detector P1, changing its energy acceptance to 36–160 MeV.

The simulation with ENIGMA indicates that the expected proton energies at forward angles are considerably higher than the acceptance of detector P2. Therefore, we installed lead absorbers up to a thickness of 12 mm in front of detector P2 to match its acceptance with the expected proton-energy spectrum of the (e, e′pp) data. The loss of solid-angle and detection efficiency introduced in this way was determined from a Monte Carlo simulation which will be discussed in the next subsection.

2.4. Reconstruction of particle momenta and calibration of proton detectors

The electron four-vector at the interaction point is reconstructed from the information of the QDQ spectrometer using transport matrix elements in a well-established formalism [23]. The momentum resolution ($\delta p_{e'}/p_{e'} \approx 1.5 \times 10^{-4}$) and the angular resolutions ($\delta\theta_{e'} \approx 6$ mrad, $\delta\phi_{e'} \approx 12$ mrad) of the QDQ, obtained with a standard set of matrix elements, are sufficient for this experiment.

The determination of the proton-momentum vector involves track reconstruction, particle identification and calculation of the energy. For any given energy at the vertex, the energy deposited along the track can be calculated from the Bethe–Bloch formula [24]. Quenching of scintillation at high values of ionization density is accounted for by the phenomenological formula of Wright [25]. Formulas for conversions between light, energy loss and proton energy at the vertex have been evaluated numerically and parametrized for each detector geometry.

The hodoscope elements have been calibrated by means of protons with energies of up to 100 MeV by employing the over-determined kinematics of the ^{1}H(e, e′p) reaction. Also, the conversion formulas have been checked with these calibration data. The amounts of scintillation light produced in two successive layers were used to calibrate all layers behind the hodoscope and to perform particle identification in the off-line analysis. The energy resolution resulting from this procedure amounts to 1.9 and 3.3 MeV FWHM for the energy ranges 27–37 and 75–100 MeV, respectively.

The measured coincidence times are corrected for four effects: time-of-flight of the particles, light propagation in the scintillators, phase differences between the elements of each detector trigger and time walk introduced by the discriminators. The resulting time resolution for electron–proton coincidences typically amounts to 1 ns FWHM.

The reduction of solid-angle and detection efficiency of the proton detectors, due to multiple scattering and hadronic interactions, has been assessed from Monte Carlo simulations with the code GEANT [26]. To simulate the effect of dead time in the detector channels, the simulated tracks are converted to pseudo-data by an intermediate code with the dead times as measured during the experiment as input [27]. The energy acceptance and the solid angle averaged over this acceptance are given in Table 1 as a function of the thickness of the lead placed in front of the detector.

2.5. Electronics and data acquisition

The task of the coincidence logic is to define a master event trigger (MET) which starts the timing measurements and latches the data buffers. The arm-trigger signals

Table 1
Dynamic acceptances ΔT_p of the proton detectors and averages $\overline{\Omega}$ of the solid angles over the ΔT_p for each total thickness of Pb absorber plates applied in the experiment. In the actual analysis (see Section 3) two T_p-dependent efficiency functions in combination with fixed geometrical solid angles are used instead of the averages $\overline{\Omega}$

Reaction	Proton detector	Thickness [mm]	ΔT_p [MeV]	$\overline{\Omega}$ [msr]
(e, e′p)	P1	1	36–160	27.1
(e, e′pp)	P1	1	36–160	31.4
(e, e′pp)	P2	3	58–204	27.7
		6	74–211	25.2
		9	88–218	25.0
		12	101–225	27.8

from the proton detectors P1 and P2 and from the electron detector QDQ serve as inputs for this logic. The MET signal is formed by the logic OR of three subtriggers: (i) a double coincidence between QDQ and P1, (ii) a double coincidence between QDQ and P2, and (iii) a triple coincidence between QDQ, P1 and P2. The MET signal starts a number of TDCs, which are stopped by the individual arm triggers and, for redundancy, by the coincidence subtriggers.

The detector data that belong to an MET are retrieved from their buffers and merged into one data stream which is stored on mass-storage devices. Scalers allow to monitor the circuitry at various levels and to calculate dead times.

3. Analysis

The analyses of the (e, e′p) and (e, e′p) data are to a great extent identical. The main difference lies in the subtraction procedure for accidental coincidences. First, in Subsection 3.1, the analysis procedure of the double-coincidence data is described. In Subsection 3.2, this is done for the triple-coincidence data, with emphasis on the extraction of cross sections from low-statistics data.

3.1. $^{12}C(e, e'p)$

The experimental six-fold differential cross section of the double-coincidence reaction $^{12}C(e, e'p)$ is determined from

$$\sigma_d(E_m, p_m) \equiv \frac{d^6\sigma}{d\Omega_{e'}\, d\Omega_p\, dE_{e'}\, dT_p} = \frac{N_d(E_m, p_m)}{V_d(E_m, p_m)\eta(T_p)\int L(t)\, dt} \tag{3}$$

where N_d represents the number of true (e, e′p) events, V_d the detection volume in phase space, η the efficiency of proton detection and L the luminosity. The phase-space variables missing energy, E_m, and missing momentum, p_m, are defined by

$$(E_m, p_m) \equiv (\omega - T_p, |\boldsymbol{q} - \boldsymbol{p}_p|), \tag{4}$$

where $\boldsymbol{p}_p$ and T_p are the momentum and kinetic energy of the detected proton. We refrained from accounting for the kinetic energy of the recoiling nucleus in the expression for E_m because in a multi-nucleon reaction the quantity p_m is not identical to the momentum of the recoiling nucleus, as is the case in a plane-wave description of a quasi-free (e, e′p) reaction.

The luminosity $L(t)$ integrated over the duration of a measurement is the normalization factor and equals the product of the collected beam charge and the effective target thickness. The target thickness is determined from an elastic ^{12}C(e, e′) measurement. All corrections that are constant over the detection volume (e.g. the dead time of the coincidence trigger) are included in $\int L(t)\,dt$. The function $\eta(T_p)$ describes the energy dependence of the proton-detection efficiency due to multiple scattering, hadronic interactions and dead time of scintillator channels.

The expression of the detection volume V_d in (E_m, p_m) space is

$$V_d(E_m, p_m) = \int_{\Lambda_d} \delta(E_m - E_m^*)\,\delta(p_m - p_m^*)\,d\Omega_{e'}\,d\Omega_p\,dE_{e'}\,dT_p, \tag{5}$$

where E_m^* and p_m^* are functions of the integration variables and

$$\Lambda_d = \Delta E_{e'}\ \Delta T_p\ \Omega_{e'}\Omega_p \tag{6}$$

represents the detection volume spanned by both detectors. The detection volume V_d is determined numerically via a Monte Carlo simulation:

$$V_d(E_m, p_m) = \frac{N_{mc}(E_m, p_m)\,\Lambda_d}{S_{mc}}, \tag{7}$$

where $N_{mc}(E_m, p_m)$ is the spectrum resulting from S_{mc} simulation events randomly generated within the detection volume Λ_d. In Fig. 3 a contour plot of the detection volume $V_d(E_m, p_m)$ summed over the four measurements at $\theta_1 = -80°, -96°, -108°$ and $-120°$ is shown. Only that part of the phase space where the detection volume is larger than 10% of its maximum value is accepted for further analysis.

Distributions of E_m and p_m for accidental and real coincidences are constructed from the coincidence-time (CT) spectrum, see Fig. 4. Region B contains both real and accidental coincidences. Subtraction with events from regions A and C, containing only accidentals, yields the distributions for true (e, e′p) events. Events are weighted with the width of the region from which they originate.

The experimental cross sections are listed in Table 2. The total systematical error,

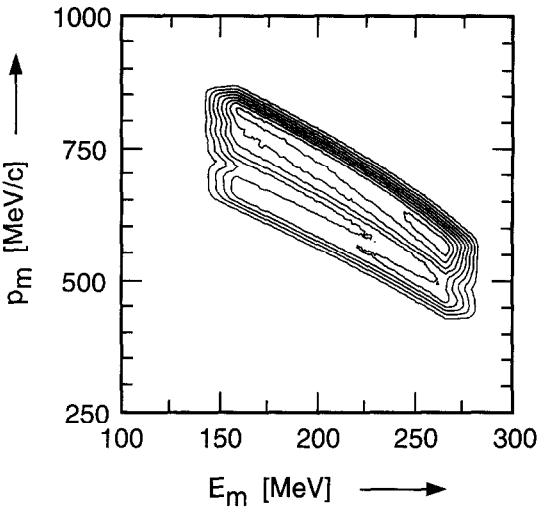

Fig. 3. Detection volume V_d in (E_m, p_m) space for the ^{12}C(e, e'p) measurements with detector P1. The contour lines are equidistant by 10% of the maximum of V_d, which is located at (265 MeV, 560 MeV/c).

which amounts to 5%, is obtained by summing the square of the individual errors. It is dominated by the uncertainties in three quantities: the target thickness (3%), the trigger efficiency of the proton detector (3%) and the efficiency function η (3%).

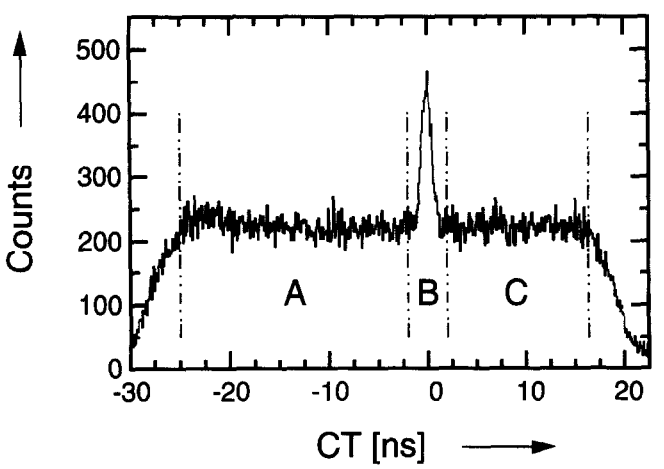

Fig. 4. ^{12}C(e, e'p) coincidence-time spectrum of data set $\theta_1 = -96°$ after application of all timing corrections. The windows for accidentals (A and C) and true-plus-accidental coincidences (B) have been placed at $(-25, -2)$ and (2, 16.4) ns and at $(-2, 2)$ ns, respectively.

Table 2
Experimental cross sections $\sigma_d(E_m, p_m)$ in 10^{-10} fm^2/(MeV·sr)^2 of the ^{12}C(e, e′p) reaction. The numbers in parentheses are standard deviations indicating the statistical error on the least-significant digit

E_m [MeV]	p_m [MeV/c]					
	435–510	510–580	580–650	650–720	720–790	790–865
150–160				1.8(4)	0.1(2)	0.3(3)
160–170			2.9(10)	1.6(4)	0.5(3)	0.0(2)
170–180			3.1(8)	2.2(4)	0.8(3)	0.7(4)
180–190			2.1(6)	1.8(4)	0.5(3)	1.6(7)
190–200			5.1(6)	2.2(5)	0.7(4)	
200–210		5.8(15)	5.1(6)	1.5(4)	1.1(5)	
210–220		6.9(10)	3.0(5)	1.7(4)	2.8(9)	
220–230		6.4(9)	3.3(5)	1.3(5)		
230–240	5(3)	6.0(7)	2.6(5)	3.6(7)		
240–250	8.9(17)	4.4(7)	3.0(6)	2.8(11)		
250–260	7.9(13)	3.6(6)	3.2(7)			
260–270	8.9(10)	4.0(7)	3.1(10)			
270–280	5.7(15)	4.4(11)	4(2)			

3.2. $^{12}C(e, e'pp)$

The nine-fold differential cross section for the (e, e′pp) reaction can be expressed as

$$\sigma_t(\gamma_{p1}, \gamma_{p2}, E_{2m}) \equiv \frac{d^9\sigma}{dE_{e'}\, dT_{p1}\, dT_{p2}\, d\Omega_{e'}\, d\Omega_{p1}\, d\Omega_{p2}}$$

$$= \frac{N_t(\gamma_{p1}, \gamma_{p2}, E_{2m})}{V_t(\gamma_{p1}, \gamma_{p2}, E_{2m})\eta_1(T_{p1})\eta_2(T_{p2})\int L(t)\, dt}, \tag{8}$$

where the subscript t stands for true three-fold coincidences. The double-missing energy E_{2m} is defined by

$$E_{2m} = \omega - T_{p1} - T_{p2}, \tag{9}$$

and the angle γ_{p1} (γ_{p2}) is the emission angle of the proton detected by detector P1 (P2) relative to the momentum transfer, calculated in the lab-frame.

Due to the low statistical accuracy the data will be presented after integration over the E_{2m} variable. Moreover, the granularity of γ_{p1} (γ_{p2}) is reduced to the angle γ_1 (γ_2) between the momentum transfer and the central axis of detector P1 (P2). The experimental cross section, averaged over the solid angles of the electron spectrometer and the two proton detectors, can then be written as

$$\sigma_t(\gamma_1, \gamma_2) \equiv \int \sigma_t(\gamma_1, \gamma_2, E_{2m})\, dE_{2m}$$

$$= \frac{1}{\Omega_{e'}\Omega_{p1}\Omega_{p2}\int L(t)\, dt} \int \frac{N_t(\gamma_1, \gamma_2, E_{2m})}{V_t(E_{2m})\eta_1(T_{p1})\eta_2(T_{p2})} dE_{2m}. \tag{10}$$

Table 3
Experimental cross section $\sigma_t(\gamma_1, \gamma_2)$ of the $^{12}C(e, e'pp)$ reaction in the double-missing-energy interval $20 < E_{2m} < 120$ MeV. The numbers in parentheses are standard deviations indicating the statistical error on the least significant digit

Angles of proton detectors P1 and P2				Integrated luminosity $\int L(t)\,dt$ [C·mg/cm^2]	Eight-fold differential cross section $\sigma_t(\gamma_1, \gamma_2)$ [10^{-11} fm^2/(MeV^2·sr^3)]
θ_1 [deg]	γ_1 [deg]	θ_2 [deg]	γ_2 [deg]		
−80	−95	55	40	2.3	6(3)
−96	−111	55	40	3.2	3(2)
−108	−123	90	75	0.5	1(7)
−120	−135	55	40	1.2	11(3)

The energy-dependent detection probabilities are given by the denominator of the integrand in Eq. (10). The detection volume $V_t(E_{2m})$ is given by

$$V_t(E_{2m}) = \int_{A_t} \delta(E_{2m} - E^*_{2m})\, dE_{e'}\, dT_{p1}\, dT_{p2}, \tag{11}$$

where E^*_{2m} is a function of the electron energy $E_{e'}$ and the proton energies T_{p1} and T_{p2} according to Eq. (9) and the integral is taken over the energy acceptances of the three detectors:

$$A_t = \Delta E_{e'}\ \Delta T_{p1}\ \Delta T_{p2}. \tag{12}$$

The integral of Eq. (11) has been evaluated numerically. The proton-detection efficiencies are described by the functions $\eta_1(T_{p1})$ and $\eta_2(T_{p2})$.

In triple-coincidence measurements five categories of coincidence events exist. Besides the true triple-coincidences (T) and three-fold accidental coincidences (R_0) there are three different types of true double-coincidences which are accidentally coincident with a third particle (R_1, R_2 and R_3). The coincidence times CT_1 and CT_2 (electron-detector QDQ relative to proton detectors P1 and P2, respectively) contain the information to separate these five contributions. Coincidences of type R_1, R_2 and R_3 appear as bands in a scatter plot of CT_1 versus CT_2, R_0 gives rise to a flat background and T is located where R_1, R_2 and R_3 intersect.

A fit to the two-dimensional coincidence-timing spectrum yields an accurate separation of the contributions by accidental and true (e, e'pp) events. The fit function is a sum of a flat background and of four gaussians, each described by an amplitude, a width and a centroid. The data sets for the three values of γ_1 were mutually linked by common width and centroid parameters in the fit functions.

The density of events in the (CT_1, CT_2) time domain amounts to roughly 1 ns^{-2}. Sorting the data in bins that are on the order of the experimental resolution prior to a fit would incur a serious loss of precision. Therefore, the timing spectra were not binned. The procedure for fitting unbinned spectra which are governed by Poisson statistics is based on an extension of the maximum-likelihood theory [28]. The determination of the

number of (e, e'pp) events has been discussed in Ref. [29]. [4] Here, we explicitly included the energy dependence of the detection probability in the fit procedure.

The experimental cross sections, evaluated over the missing-energy interval between 20 and 120 MeV, are given in Table 3. The result for the kinematics with $\theta_1 = -108°$ and $\theta_2 = 90°$ is consistent with zero, which is expected because this kinematics is far off the back-to-back condition. The propagation of statistical and systematical errors is similar to that in the ^{12}C(e, e'p) data. The quadratic sum of all contributions results in a total systematic error of 7%, which is small compared to the statistical error.

4. ^{12}C(e, e'p): discussion of experimental results

This section starts with a comparison with other (e, e'p) measurements performed in similar kinematical conditions. The importance of radiative effects and final-state interactions (FSI) is estimated in Subsections 4.2 and 4.3, respectively. In a discussion of the measured data we employ in Subsection 4.4 an event generator which uses some basic prescriptions of the reaction dynamics. In Subsection 4.5, experimental missing-energy spectra are compared with those of a microscopic model for virtual-photon coupling to pion-exchange and Δ-currents.

4.1. Comparison with other measurements

Baghaei et al. have measured the ^{12}C(e, e'p) reaction in the Δ-excitation region with electron kinematics comparable to that of our experiment [10]. The corresponding values of the virtual-photon polarization, defined as $\varepsilon = [1 + 2\tan^2(\frac{1}{2}\theta_{e'})/(1 - \omega^2/|\boldsymbol{q}|^2)]^{-1}$, are approximately equal; $\varepsilon = 0.62$ (present work) and $\varepsilon = 0.57$ (Ref. [10]). The latter experiment covers a large range of missing energy, $E_m = 0$–320 MeV, but did not cover missing momenta larger than $p_m = 450$ MeV/c as protons were detected parallel to the momentum transfer. The structure in the missing-energy spectrum at $E_m > 160$ MeV is consistent with pion production. The authors suggest that quasi-free knockout of a two-nucleon system, $\gamma^* + \text{``pN''} \rightarrow p + N$, is responsible for the response below the pion-production threshold. The cross sections measured in the present experiment vary between 0.2×10^{-10} and 10×10^{-10} fm^2/(MeV · sr)^2. The multi-nucleon response in kinematics II of Ref. [10], peaking at $E_m \approx 100$ MeV, amounts to 2.5×10^{-10} fm^2/(MeV · sr)^2.

Takaki [30] has calculated semi-exclusive (e, e'p) cross sections taking into account the contributions from two- and three-nucleon emission in the zero-range assumption and real-charged-pion production followed by two- or three-nucleon emission. He found that in the dip region three-nucleon processes peak in parallel kinematics. Relative to

[4] For full consistency between the definitions of the likelihood function Ξ and the standard deviation the errors in that paper must be reduced by a factor $\sqrt{2}$

two-nucleon emission, three-nucleon processes gain in importance at larger proton angles and at energy transfers compatible with Δ-excitation.

4.2. Radiative effects

The effects of bremsstrahlung on (e, e'p) measurements and the way to correct the data for this effect are well documented [31,32]. Internal bremsstrahlung, which is the emission of a photon just before or after the electron-scattering process, dominates. The effect of external bremsstrahlung is negligible with the target thickness used. We apply the peaking approximation: the photon is emitted in the direction of the radiating electron either incoming or outgoing. In case bremsstrahlung has occurred, the nuclear response is probed at lower missing energies than reconstructed from the experimental variables $(\omega, \boldsymbol{q})$ and $\boldsymbol{p}_p$, see Eq. (4). The corresponding difference between the calculated missing momentum and the one actually probed depends on the particular kinematics and on whether bremsstrahlung has occurred before or after the scattering process.

In Fig. 5 the kinematically allowed paths for bremsstrahlung are drawn for the two extremes and the centre of the measured phase space. The end points at $E_m = 160$, 210 and 260 MeV can be fed by the points at lower E_m along either curve. Although the probability of photon emission with high energies E_γ is low, internal bremsstrahlung can be a nonnegligible component of the measured cross section if the nuclear response increases rapidly with decreasing missing energy. The fact that the paths in Fig. 5 do not stay within the detection volume precludes a self-consistent radiative correction of the

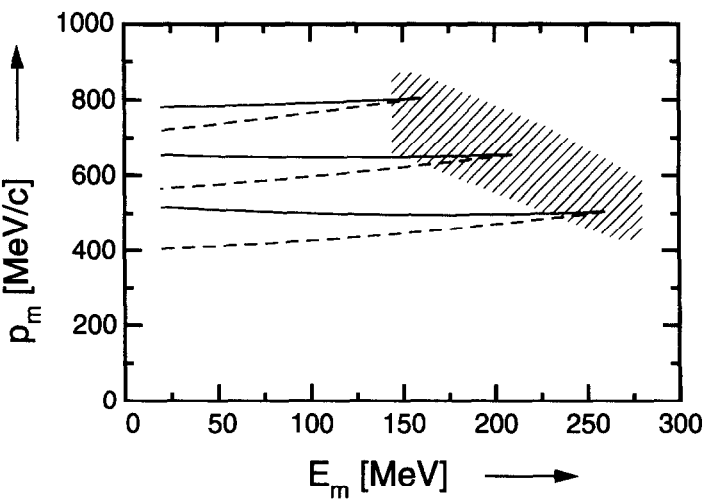

Fig. 5. Propagation paths of the radiative effect towards the extremes and the centre of the measured part of the (E_m, p_m) plane. Dashed and solid curves correspond with radiating before and after the electron-scattering process, respectively. The shaded area represents the part of the phase space that is covered by the detection volume of the present experiment.

data. Instead, an estimate is made of the radiative contribution from the nuclear response at low missing-energy values. The $1p_{3/2}$ and $1s_{1/2}$ momentum distributions of ^{12}C are assumed to be located at a removal energy of 16 and 35.5 MeV, respectively. They have been calculated up to $p_m = 800$ MeV/c with correlated quasi-particle (CQP) wave functions, by which the depletion of states below the Fermi level is effectively taken into account [4]. In order to account for FSI effects these theoretical momentum distributions are shifted over -30 MeV/c and are multiplied by 0.4, such that they describe data measured between $p_m = 0$ and 225 MeV/c [20] and between 375 and 600 MeV/c [33]. Comparison with other calculated momentum distributions using a Woods–Saxon potential or the generator coordinate method [34] shows that the CQP estimate is a clear upper limit.

The largest radiative contribution, both relative and absolute, occurs in the high-E_m, low-p_m part of the experimentally covered phase space and amounts to 9% of the observed strength. For the low-E_m, high-p_m part a value smaller than 1% is found. This can qualitatively be explained as follows: the decrease of the $1p_{3/2}$ and $1s_{1/2}$ momentum distributions is not completely compensated by a sufficient increase in probability of the radiative effect over the corresponding smaller missing-energy distances E_γ.

A self-consistent procedure for the radiative unfolding of spectra is only possible if the origin of all contributing radiative processes is covered by the experiment. Since no data or model calculations are available for the (e, e′p) response above the two-particle-emission threshold, our estimate of the radiative effect remains a lower limit.

4.3. Nucleon rescattering

After a nucleon has been struck by the virtual photon it may interact with the residual nucleus. In semi-exclusive (e, e′p) experiments these final-state interaction effects can cause strength, which is removed at low (E_m, p_m), to show up in the whole (E_m, p_m) phase space. The extent to which FSIs redistribute strength from below the two-particle-emission threshold to the continuum may be quite large, depending on the kinematics of the experiment. Due to the lack of models with which the redistribution of continuum strength can be calculated, we limit ourselves here to the effect of nucleon rescattering on strength that originates from below the two-particle-emission threshold.

Several phenomenological approaches have been applied to calculate rescattering effects in quasi-elastic knockout reactions in parallel kinematics [35–37]. An estimate for this experiment has been made with the code MulScat, in which the nucleon–nucleus reaction is described by a cascade of particle–particle collisions [36]. The channel (e, e′p) (p, p′) is the first-order contribution of FSI to the electron–proton coincidence measurement and involves both the direct and the exchange process. The charge-exchange process (e, e′n) (n, p) has not been taken into account because of the ratio of electron–proton and electron–neutron cross sections: $\sigma_{ep}/\sigma_{en} \approx 10$. Input to the calculation are the harmonic-oscillator (HO) momentum distributions for the 1p and 1s shells (with HO constant $b = 1.7$ fm) and σ_{ep}.

Since only values of the initial proton momentum $|\boldsymbol{k}_p| > 450$ MeV/c are accessible in the present kinematics, the rescattering cross section must be scaled up by a number that represents the ratio between the HO and more realistic momentum distributions. The ratio of the CQP and HO momentum distributions at $|\boldsymbol{k}_p| = 450$ MeV/c is ≈ 100. The choice of this number as the scaling factor is motivated by three facts: (i) CQP momentum distributions are an upper limit for $|\boldsymbol{k}_p| > 400$ MeV/c (see Section 4.2). (ii) As a function of γ_0, which is the angle between the initial proton momentum $\boldsymbol{k}_p$ and the momentum transfer $\boldsymbol{q}$, the (e, e′p) cross section drops faster than the (p, p′) cross section increases. (iii) Rescattering at $\gamma_0 \approx 0°$ and $|\boldsymbol{k}_p| = 450$ MeV/c followed by large-angle (p, p′) scattering dominates the cross section. For all kinematical settings of this experiment it is estimated that less than 10^{-4} of the measured cross section in the continuum is due to rescattering of protons originating from the orbits near the Fermi level.

4.4. Monte Carlo simulation

Various reaction channels may contribute to the (e, e′p) response. In the first place there is the quasi-elastic proton-knockout process (e, e′p). Secondly, there are the reactions in which two hadrons are emitted: (e, e′pN) and (e, e′pπ). Also reactions in which more than two hadrons are emitted can contribute.

We have used the Monte Carlo event-generator code ENIGMA [19], which works in a plane-wave framework, to study the relative importance of these channels. The code offers the possibility to introduce some ad hoc (e, e′p)NN and even higher multi-nucleon generators. Here we limit ourselves to the processes quasi-free (e, e′p), (e, e′pN) and (e, e′pπ), where π is either a negative or a neutral pion. Events are generated by convoluting an elementary process on a nucleon or a quasi-deuteron with the Fermi motion of the interacting system within the ^{12}C nucleus. As elementary cross sections we use the Rosenbluth formula for ^{1}H(e, e′p) and the Dressler formalism [38] for pion production. The (e, e′p)n cross section is estimated from the (γ, pn) photo-dissociation strength as parametrized by Rossi et al. [39]. The number of quasi-deuterons in ^{12}C is taken from a parametrization due to Tavares et al. [40]. We neglect the (e, e′p)p channel, because measurements with real photons of 200–300 MeV on ^{12}C show a ratio of 1 : 10 for the (γ, pp) with respect to the (γ, pn) channel [7]. The Fermi motion is accounted for by choosing a momentum distribution with parameters determined by fitting to ^{12}C(e, e′p) results in the range $p_m = 0$–600 MeV/c [20,33]. Except for this parametrized momentum distribution, the model is absolutely normalized and contains no free parameters. The dynamics of the reaction is assumed to involve the uncorrelated motion of the nucleus in the initial state and an isotropic decay of the pn-system in the final state.

The simulation shows that in our kinematics, where the proton is detected in the backward hemisphere with respect to the momentum transfer $\boldsymbol{q}$, the contributions of the (e, e′p)π and the exclusive (e, e′p) channels are negligible. The contribution of single-proton knockout is extremely low because at large proton angles the nuclear response is

probed at large initial proton momenta. In the pion-production case, momentum balance is achieved due to the presence of the pion, but the Lorentz transformation between the centre-of-mass and the lab-frame will affect the direction of the slower proton more than that of the faster pion, resulting again in a strongly forward (along q) peaked emission of the proton. Since the kinematics of our experiment rules out quasi-free one-nucleon knockout and suppresses pion production, we assert that we have measured mostly multi-nucleon knockout.

4.5. Microscopic model for coupling to two-body pion exchange and Δ-currents

The contribution from two-nucleon knockout to the semi-exclusive ^{12}C(e, e′p) cross section, due to coupling of the virtual photon to two-body currents generated by meson exchange and intermediate Δ-excitation, is calculated in an unfactorized microscopic approach by Ryckebusch et al. [41]. In this model the semi-exclusive amplitude is obtained by integrating the (e, e′pn) and (e, e′pp) strengths over the unobserved hadron. Only coupling of the virtual photon to transverse two-body currents is considered. All diagrams, both resonant and nonresonant, in which one pion is exchanged are taken into account.

For the MEC contribution a nonrelativistic reduction of the one-pion-exchange-potential (OPEP) current operators is taken. The Δ-contribution is calculated using a nonstatic Δ-current operator. The standard dipole form factor is chosen for the electromagnetic form factors, while for the strong πNN form factor a monopole form with a cutoff mass of 1200 MeV is used. In addition to the two-nucleon knockout contribution, also the contribution from pion production to the semi-exclusive (e, e′p) spectrum has been calculated. In the model both the (e, e′pπ^-) and (e, e′pπ^0) channel are considered. The unitary pion electroproduction model – in which the calculations were performed – takes into account both resonant and nonresonant diagrams. The dominant transverse contribution was checked to give an accurate description of both the multipoles and the angular distributions of the pion-photoproduction process on a free nucleon up to photon energies of 400 MeV [42]. In the two-nucleon knockout calculations, distortions of the outgoing nucleons due to interaction with the residual $(A-2)$ nucleus are taken into account via a partial wave expansion [12]. In the (e, e′pp), (e, e′pn) and (e, e′pπ) model calculations, proton and neutron removal from all possible shell combinations is considered. The bound-state single-particle wave functions are obtained via a Hartree–Fock calculation using an effective interaction of the Skyrme type.

In Fig. 6 the cross sections, measured at the proton emission angles $-80°$ and $-120°$, are compared with the predictions of this model. The calculated strengths from the pp-, pn- and pπ-channels are shown. It is clear that the two-nucleon knockout process gives a major contribution to the lower and middle part of the missing-energy spectrum. The direct-pion-production process is seen to produce a strong rise at the highest E_m values. As direct pion production is a one-body process, it is far more important at forward than at backward proton angles. Fig. 6 shows that in the middle part of the missing-energy spectrum the measured strength is a factor 1.5 to 3 larger than

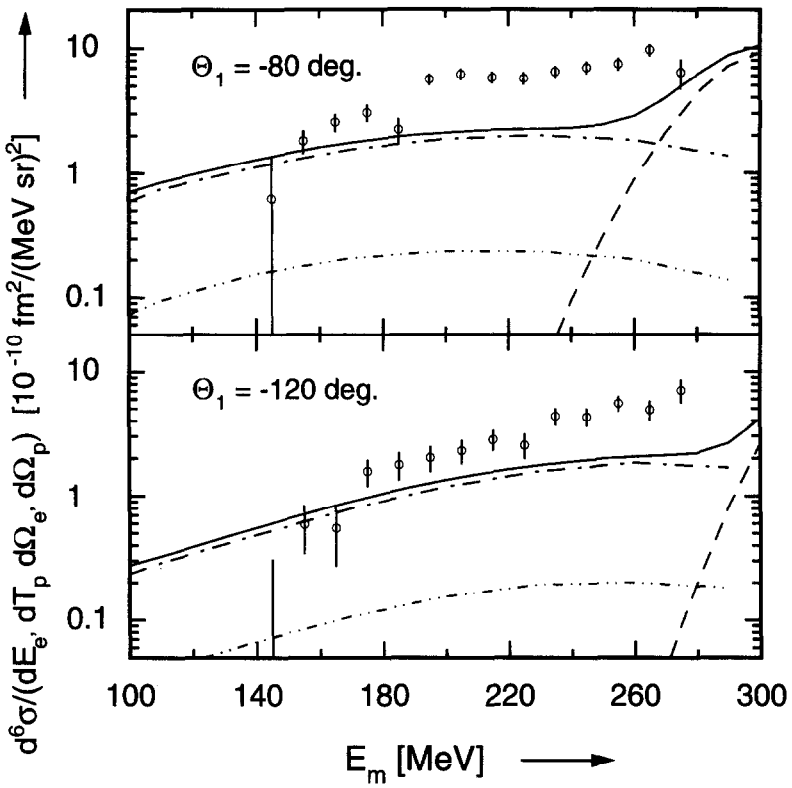

Fig. 6. Six-fold differential cross section of the reaction ^{12}C(e, e′p) versus missing energy for proton-emission angles −80° (top) and −120° (bottom). The double-dot-dashed, dot-dashed, dashed and solid curves correspond to the pp, pn, pπ and (pp + pn + pπ) cross-section predictions, respectively [12,42,49].

the calculated strength obtained from an incoherent sum of the processes considered here. A similar type of comparison performed for the ^{12}C(γ, p) reaction at $E_\gamma = 300$ MeV confirms these findings. Based on the arguments outlined in Refs. [30,43], it is suggested that a two-step mechanism could be responsible for the strength in this intermediate missing-energy region. In line with the results of the calculations of Ref. [43] for the real photon case, we expect that in this two-step mechanism a pion is first produced on a nucleon; its subsequent absorption on a nucleon pair then leads to multi-nucleon knockout. Estimations of the strength of this process are under way [42].

5. ^{12}C(e, e′pp): model calculation and experimental results

The present data for the ^{12}C(e, e′pp) reaction are compared with the results of a theoretical approach for two-nucleon knockout which was proposed and applied to both electro- and photo-induced reactions [15,44]. The theoretical framework is outlined in Subsection 5.1. The results of the calculation are presented in Subsection 5.2 and compared with experimental data in Subsection 5.3.

5.1. Theoretical framework

In the one-photon-exchange approximation and neglecting the distortion produced by the nuclear Coulomb field on the incident and the outgoing electrons, the triple-coincidence (e, e'NN) cross section is given by the contraction of a leptonic tensor with a hadronic tensor. The leptonic tensor only contains the kinematical variables of the electron. The components of the hadronic tensor are given by products of the Fourier transforms of the matrix elements of the nuclear charge-current density operator taken between initial and final nuclear states. Assuming a direct-knockout mechanism and a transition to a specific final state of the residual nucleus, they can be written as

$$J^{\mu}(\boldsymbol{q}) = \int \psi_{\mathrm{f}}^{*}(\boldsymbol{r}_1, \boldsymbol{r}_2) J^{\mu}(\boldsymbol{r}, \boldsymbol{r}_1, \boldsymbol{r}_2) \psi_{\mathrm{i}}(\boldsymbol{r}_1, \boldsymbol{r}_2)\, \mathrm{e}^{i\boldsymbol{q}\cdot\boldsymbol{r}}\, \mathrm{d}\boldsymbol{r}\, \mathrm{d}\boldsymbol{r}_1\, \mathrm{d}\boldsymbol{r}_2. \tag{13}$$

The integrand in Eq. (13) contains three ingredients: the two-nucleon overlap integral ψ_{i}, the nuclear current operator J^{μ} and the final-state wave function ψ_{f}.

The overlap integral ψ_{i} is the spectroscopic amplitude and also contains the spectral strength that gives the probability of removing two nucleons from the target nucleus leaving the residual nucleus in the selected final state. Usually, ψ_{i} is written as the product of the pair function of the shell model, given by the product of two uncoupled single-particle wave functions belonging to the same shell, and of a correlation function of Jastrow type. This correlation function depends on the radial parameter c, which is related to dynamical correlations at short distances. To reduce the complexity of the calculations, spin and isospin couplings are neglected and antisymmetrization is fulfilled by means of suitable spin and isospin projection operators. As the approach cannot distinguish different pairs of nucleons coming out of the considered shell, the calculated response contains a sum over all of them. In the correlation function only the central part is considered. It weighs the overlap between the single-particle wave functions with a probability that the two particles are in close proximity of each other. This approach takes the short-range part of the NN-interaction in a phenomenological way into account.

The final-state wave function ψ_{f} contains FSI effects, which are in principle both due to the mutual interaction between the two ejected nucleons and due to the interaction of each one of the nucleons with the residual nucleus. In the considered approach the mutual interaction is neglected. Such an approximation is expected to be reasonable if the two nucleons are ejected in opposite directions and with large enough relative momentum, a condition which is fulfilled in the present experiment. The scattering state is thus written as the product of two distorted single-particle wave functions that are taken as eigenfunctions of a phenomenological optical potential of which only the central term is retained.

The nuclear current J^{μ} is the sum of a one-body and a two-body part. The two-body component is derived performing a nonrelativistic reduction of the lowest-order Feynman diagrams. For a pp-pair, meson-exchange currents vanish and only diagrams with intermediate Δ-isobar configurations contribute. The corresponding expression of the two-body current can be found in Ref. [44].

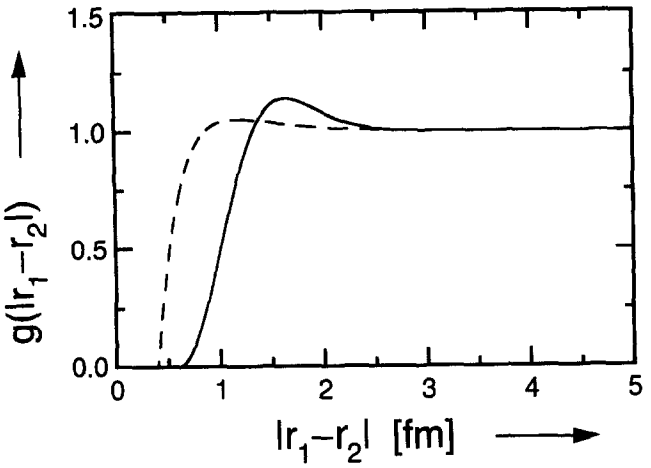

Fig. 7. Correlation functions corresponding to a hard-core radial parameter of the NN-interaction of $c = 0.6$ fm (solid curve [46]) and $c = 0.4$ fm (dashed curve [47]), respectively. No short-range correlations are generated if the correlation function $g(|\boldsymbol{r}_1 - \boldsymbol{r}_2|)$ equals 1.

5.2. Calculation

Calculations have been performed for the two correlation functions, $g(|\boldsymbol{r}_1 - \boldsymbol{r}_2|)$, shown in Fig. 7 [15,44]. They were obtained from a variational many-body calculation for ^{16}O using different NN-interactions [45]. The radial extension of the hard-core part

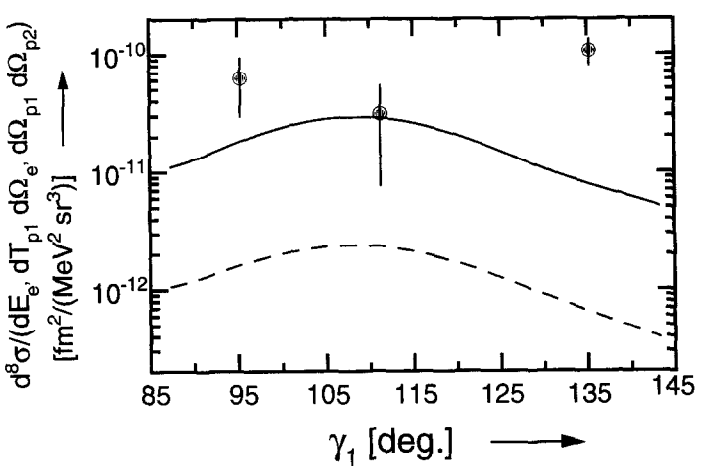

Fig. 8. Theoretical and experimental cross sections versus the angle γ_1 between the momentum transfer and the backward-emitted proton. The solid and dashed curves are the (e, e'pp) cross sections for $(1p)^2$ knockout from a fully occupied 1p shell, calculated with the radial parameter $c = 0.6$ and 0.4 fm, respectively. The three data points represent the measured cross sections of the ^{12}C(e, e'pp) reaction; besides covering $(1p)^2$ knockout, the missing-energy range also includes contributions from (1p)(1s) and $(1s)^2$ knockout. The error bars indicate the standard deviation due to statistics.

where $g = 0$ gives an adequate identification of the correlation function. The prescription given by Omhura, Morita and Yamada [46] results in a value 0.6 fm for this radial parameter. Use of the potential of Kallio and Kolltveit [47] yields the value 0.4 fm.

In the model only the two-proton knockout from a fully occupied 1p shell is considered. For the optical potential the values of Comfort and Karp have been adopted [48]. The electron kinematics is chosen equal to the experimental one, which corresponds to an invariant mass ($W \equiv [(\omega + m_N)^2 - q^2]^{1/2}$) of 1.20 GeV. This value is close to that of the peak of the Δ-resonance ($W = m_\Delta = 1.23$ GeV). The double-missing energy E_{2m}, corresponding with the binding energy of two $p_{3/2}$ protons in ^{12}C, is fixed at 27.2 MeV. The angle of the forward-detected proton is fixed at $\gamma_2 = 40°$ and the two protons are kept in coplanar kinematics with the scattered electron. Apart from taking averages over the energy acceptance of the backward proton detector, no correction for finite-acceptance effects is applied.

The calculated contributions from the sum of the one-body current, generated by proton–proton correlations, and the two-body current, accounting for pionless Δ-decay, are shown in Fig. 8. The two cross sections have the same shape but the results show a large sensitivity to the choice of the radial parameter c of the correlation function. For $c = 0.6$ fm the cross section is about one order of magnitude larger than for $c = 0.4$ fm. Also, the role of the one- and two-body currents is different in the two situations. In the case $c = 0.4$ fm the one- and two-body contributions are approximately equal, whereas the former is a factor of 20 larger than the latter in the case $c = 0.6$ fm [44]. In the present approach the two-body current is treated independently of the adopted correlation function. The dependence between the proton–proton correlation function and the two-body current deserves further investigation.

5.3. Experimental results and discussion

The results of the ^{12}C(e, e′pp) measurements in which the protons are ejected in directions close to the back-to-back correlation (see Table 3) are shown in Fig. 8. The total number of true (e, e′pp) events of these three data points amounts to 19 ± 6. Applying the criterion for statistical significance shows that this experiment has succeeded in measuring a 3σ effect for two-proton knockout. However, we cannot establish any enhancement at the conjugate angle. The limited statistical accuracy has forced us to integrate over the missing-energy range 20–120 MeV. As a consequence we are not able to distinguish $(1p)^2$, (1p)(1s) and $(1s)^2$ two-proton knockout from ^{12}C and to make a quantitative comparison with the theoretical predictions. In the model calculation a fully occupied 1p shell is assumed while the data contain contributions of knockout from all three shell combinations. Therefore, only a qualitative comparison is possible. The data seem to favour the model calculation with $c = 0.6$ fm.

6. Summary and conclusions

Cross sections for the semi-exclusive ^{12}C(e, e′p) reaction have been determined at four different proton-emission angles. Estimates of radiative effects indicate that at most

9% of the observed strength can be attributed to radiative contributions from the process in which a proton is knocked out of the 1p or 1s shell, while leaving the residual nucleus in a bound state. Phenomenological Monte Carlo calculations show that the contributions to the cross section from (non)resonant pion production and nuclear rescattering from discrete states are negligible, because the proton was detected in a direction approximately antiparallel to the three-momentum transfer $\boldsymbol{q}$.

An unfactorized microscopic calculation of transverse coupling of the virtual photon to two-body currents generated by meson exchange, intermediate Δ-excitation and pion production, gives a reasonable account of the shape of the (e, e'p) data up to $E_m = 220$ MeV. The measured cross sections are underestimated by a factor 1.5 to 3. The process in which a pion is produced on one nucleon and subsequently reabsorbed by a nucleon pair in the nucleus might account for this discrepancy.

The ^{12}C(e, e'pp) reaction cross section was measured for three combinations of proton-emission angles. The data were analyzed by a newly developed procedure for the subtraction of accidental coincidences based on the method of extended maximum likelihood. The total number of triple-coincidence events of the three kinematical settings amounts to 19 ± 6. Due to the limited statistics no final states in the $(A-2)$ system could be identified in the missing-energy spectrum. The experimentally determined triple-coincidence cross sections favour the results of a calculation in which short-range correlations are taken into account via a correlation function with a radial parameter of $c = 0.6$ fm, as well as meson exchange and delta excitation.

The highly segmented proton scintillation detectors used here, with their reasonably large solid angle and large dynamical range, have proven to be instrumental for studies of this kind using a 1% duty-factor electron beam at a peak luminosity of 2×10^{37} nucleons $\cdot$ cm$^{-2} \cdot$ s^{-1}. The results of this exploratory study have shown to be helpful in planning (e, e'pp) experiments at the presently available high-duty-factor intermediate-energy electron beams, where the second generation (200 and 500 msr) of scintillation detectors of this type will be used. These experiments will yield high-statistics triple-coincidence data in the dip and Δ-excitation regions. In combination with angular- and energy-correlation patterns, predicted by more refined theoretical models, we expect to gain a better understanding of the pp-correlation function and other multi-nucleon effects in the nuclear medium in the near future.

References

[1] P. Barreau et al., Nucl. Phys. A 402 (1983) 515.
[2] J.H. Koch, Modern topics in electron scattering, eds. B. Frois and I. Sick (World Scientific, Singapore, 1991) p. 28.
[3] R. Schiavilla et al., Nucl. Phys. A 473 (1987) 267.
[4] V.R. Pandharipande, Nucl. Phys. A 497 (1989) 43c;
D.S. Lewart, V.R. Pandharipande and S.C. Pieper., Phys. Rev. B 37 (1988) 4950.
[5] S.C. Pieper, R.B. Wiringa and V.R. Pandharipande, Phys. Rev. Lett. 64 (1990) 364.
[6] P.J. Mulders, Nucl. Phys. A 459 (1986) 525.
[7] M. Kanazawa et al., Phys. Rev. C 35 (1987) 1828.

[8] I.J.D. MacGregor et al., Nucl. Phys. A 533 (1991) 269.
[9] C. Marchand et al., Phys. Rev. Lett. 60 (1988) 1703.
[10] H. Baghaei et al., Phys. Rev. C 39 (1989) 177.
[11] O. Benhar, A. Fabrocini and S. Fantoni, Proc. Workshop on Two nucleon emission reactions, Elba 1989, eds. O. Benhar and A. Fabrocini (ETS Editrice, Pisa, 1990) p. 49.
[12] J. Ryckebusch, M. Vanderhaeghen, L. Machenil and M. Waroquier, Nucl. Phys. A 568 (1994) 828.
[13] J.M. Laget, Phys. Rev. C 35 (1987) 832.
[14] J.M. Laget, New vistas in electronuclear physics, eds. E. Tomusiak et al. (Plenum, New York, 1986) p. 361; Phys. Lett. B 151 (1985) 325.
[15] C. Giusti and F.D. Pacati, Nucl. Phys. A 535 (1991) 573.
[16] A. Altman et al., Phys. Rev. Lett. 50 (1983) 1187.
[17] F. Adimi et al., Phys. Rev. C 45 (1992) 2589.
[18] J.W. Lightbody Jr. and J.S. O'Connell, Comput. Phys. 2 (1988) 57.
[19] J.L. Visschers, Proc. Conf. MC93 on Monte Carlo simulations in high energy and nuclear physics, eds. P. Dragovitsch, S.L. Linn and M. Burbank (World Scientific, Singapore, 1994) p. 350.
[20] G. van der Steenhoven et al., Nucl. Phys. A 480 (1988) 547.
[21] J.H.J. Distelbrink et al., Nucl. Instr. Meth. 220 (1984) 433.
[22] A. Zondervan et al., Nucl. Instr. Meth. A 342 (1994) 436.
[23] L. de Vries, J.B.J.M. Lanen, H.P. Blok and H. de Vries, Nucl. Instr. Meth. A 292 (1990) 629.
[24] J.F. Janni, Atom. Data Nucl. Data Tables 27 (1982) 147.
[25] T.J. Gooding and H.G. Pugh, Nucl. Instr. Meth. 7 (1960) 189.
[26] R. Brun et al., GEANT3 user's guide, CERN DD/EE/84-1 (1987).
[27] M. Kelder, Master's thesis, State University of Utrecht (1993), unpublished.
[28] R. Barlow, Nucl. Instr. Meth. A 297 (1990) 496.
[29] T.P. Smith, F.W. Hersman and A. Zondervan, Nucl. Instr. Meth. A 334 (1993) 537.
[30] T. Takaki, Phys. Rev. C 39 (1989) 359.
[31] E. Quint, Ph.D. thesis, University of Amsterdam (1988), unpublished.
[32] E. Borie and D. Drechsel, Nucl. Phys. A 167 (1971) 369.
[33] L.J.H.M. Kester et al., Phys. Lett. B 344 (1995) 79.
[34] A.N. Antonov et al., Nuovo Cimento 103 A (1990) 1287;
A.N. Antonov, P.E. Hodgson and I.Zh. Petkov, Nucleon momentum and density distributions in nuclei (Clarendon, Oxford, 1988) p. 126.
[35] R.W. Lourie et al., Phys. Rev. Lett. 56 (1986) 2364.
[36] L.B. Weinstein et al., Phys. Rev. Lett. 64 (1990) 1646.
[37] G.P. Capitani et al., Nuovo Cimento 85 A (1985) 37.
[38] E.T. Dressler, Can. J. Phys. 66 (1988) 279.
[39] P. Rossi et al., Phys. Rev. C 40 (1989) 2412.
[40] O.A.P. Tavares and M.L. Terranova, J. Phys. G 18 (1992) 521.
[41] J. Ryckebusch et al., Phys. Rev. C 49 (1994) 2704.
[42] M. Vanderhaeghen and J. Ryckebusch, publication in preparation.
[43] R.C. Carrasco, M.J. Vicente Vacas and E. Oset, Nucl. Phys. A 570 (1994) 701.
[44] C. Giusti, F.D. Pacati and M. Radici, Nucl. Phys. A 546 (1992) 607.
[45] J.W. Clark, The many-body problem: Jastrow correlations versus Brueckner theory, eds. R. Guardiola and J. Ros, Lecture notes in physics, Vol. 138 (Springer, Berlin, 1981) p. 184.
[46] T. Ohmura, M. Morita and M. Yamada, Prog. Theor. Phys. 15 (1956) 222.
[47] A. Kallio and K. Kolltveit, Nucl. Phys. 53 (1964) 87.
[48] J.R. Comfort and B.C. Karp, Phys. Rev. C 21 (1980) 2162.
[49] J. Ryckebusch et al., Phys. Lett. B 333 (1994) 310.